

# Nonlinear optical spectroscopy of indirect excitons in coupled quantum wells.

P. Andreakou,<sup>1</sup> S. Cronenberger,<sup>1</sup> D. Scalbert,<sup>1</sup> A. Nalitov,<sup>2</sup> N. A. Gippius,<sup>2,3</sup> A. V. Kavokin,<sup>4,5,6</sup> M. Nawrocki,<sup>7</sup> J. R. Leonard,<sup>8</sup> L. V. Butov,<sup>8</sup> K. L. Campman,<sup>9</sup> A. C. Gossard,<sup>9</sup> and M. Vladimirova<sup>1</sup>

<sup>1</sup>Laboratoire Charles Coulomb, UMR 5221 CNRS/ Université Montpellier 2, F-34095, Montpellier, France

<sup>2</sup>Institut Pascal, PHOTON-N2, Université Blaise Pascal, CNRS, 24 avenue des Landais, 63177 Aubière Cedex, France.

<sup>3</sup>Skolkovo Institute of Science and Technology, Skolkovo, Moscow Region, 143025, Russia.

<sup>4</sup>Russian Quantum Center, 100, Novaya, Skolkovo, Moscow Region, 143025, Russia

<sup>5</sup>School of Physics and Astronomy, University of Southampton, Southampton, SO17 1BJ, United Kingdom

<sup>6</sup>Spin Optics Laboratory, St-Petersburg State University, 1, Ulianovskaya, St-Petersburg, 198504, Russia

<sup>7</sup>Institute of Experimental Physics, University of Warsaw, Hoża 69, 00-681 Warsaw, Poland

<sup>8</sup>Department of Physics, University of California at San Diego, La Jolla, CA 92093-0319, USA

<sup>9</sup>Materials Department, University of California at Santa Barbara, Santa Barbara, California 93106-5050, USA

Indirect excitons in coupled quantum wells are long-living quasi-particles, explored in the studies of collective quantum states. We demonstrate, that despite the extremely low oscillator strength, their spin and population dynamics can be addressed by time-resolved pump-probe spectroscopy. Our experiments make it possible to unravel and compare spin dynamics of direct excitons, indirect excitons and residual free electrons in coupled quantum wells. Measured spin relaxation time of indirect excitons exceeds not only one of direct excitons, but also one of free electrons by two orders of magnitude.

An exciton is a semiconductor quasi-particle formed by an electron and a hole bound by Coulomb interaction. A spatially indirect exciton (IX) can be formed in coupled quantum wells (CQWs) when an electron and a hole are confined in different quantum wells. Remarkable features of IX gases, including spontaneous coherence and condensation [1–3], long-range spin currents and spin textures [2, 3], pattern formation [3–6], and correlation phenomena [7, 8] have been recently demonstrated. The spin structure of indirect excitons is particularly interesting and important. The exciton states with spin projections  $\pm 1$  to the structure axis can couple to light to form bright states, while excitons with  $\pm 2$  spin projections are dark, and nontrivial to access by emission spectroscopy [9]. Measuring the density and polarization state of both dark and bright components of the IX gas is one of challenges in the physics of IX. Another issue is the effect of the residual two-dimensional electron gas (2DEG) in the gated CQWs on the exciton spin dynamics [5, 10]. Indeed, the 2DEG can significantly affect IX spin dynamics and other properties [11]. Traditional photoluminescence experiments fail in accessing a dilute 2DEG, while the methods of nonlinear time-resolved spectroscopy, such as pump-probe Kerr rotation and reflectivity, may bring new insights. Pump-probe techniques have been successfully applied to investigate electron [12], hole [13], direct exciton (DX) [14, 15] and exciton-polariton [16] dynamics in nanostructures. But their application to IX spectroscopy is limited, because of the extremely low IX oscillator strength. Due to this fundamental reason, studies of indirect excitons have been limited to linear optics methods until now.

In this Letter we report a proof-of-concept experiment demonstrating the potential of time-resolved pump-probe

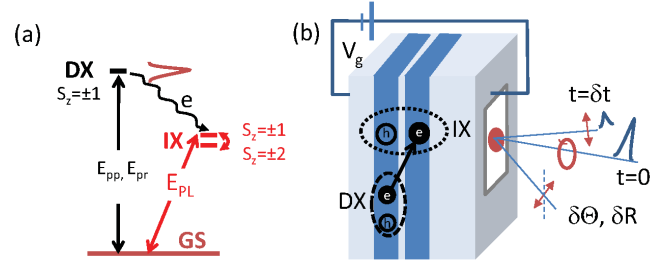


FIG. 1. (a) Three-level scheme of the pump-probe experiment with relevant excitonic states in a biased CQWs. Low oscillator strength IX states are pumped ( $E_{pp}$ ) and probed ( $E_{pr}$ ) via DX transition, through their common ground state. (b) Sketch of CQWs and pump-probe experiment.

spectroscopy of IXs in CQWs. The method is based on the three-level scheme (Fig. 1 (a)). In this scheme pump and probe light pulses are resonant with the optically active DX transition, and both bright and dark IXs are probed via their ground state, common with the DXs. The experiment reported here is the first realization of our theoretical proposal [17]. We show that both DX and IX spin and population dynamics, as well as the spin polarization of residual electrons may be detected via the modulation of reflectivity and Kerr rotation spectra at the DX resonances. From the photoinduced reflectivity measured as a function of the pump-probe delay we extract DX and IX radiative lifetimes varying from 1 to 30 ns, with a clear footprint of the gate voltage controlled DX-IX anticrossing. In the Kerr rotation signal, we unravel DX, IX and electron spin dynamics. In unbiased CQWs electron spin contribution is negligible, and the coherent dynamics of DXs dominates. In biased CQWs

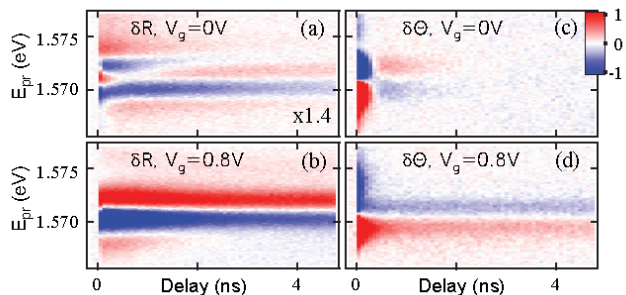


FIG. 2. Reflectivity (a, b) and Kerr rotation (c, d) induced by pump pulses resonant with DX transition ( $E_{pp} = 1.568$  eV), measured as a function of the pump-probe delay and probe energy at  $V_g = 0$  (a, c) and  $V_g = 0.8$  V (b, d).

the electron density and spin polarization build up. It appears that not only DX, but also bare electron spin relaxation is much faster ( $\simeq 200$  ps) than the spin relaxation of IXs (up to 10 ns). We show that this is due to more efficient localization of IXs. From the spectral shape analysis of the nonlinear signals we conclude that the main mechanisms of IX-DX interaction are the spin-independent narrowing of the DX resonance and the strongly spin dependent blue shift of the DX energy.

The sample we study consists of two 8 nm wide GaAs quantum wells separated by a 4 nm  $\text{Al}_{0.33}\text{Ga}_{0.67}\text{As}$  barrier and surrounded by 200 nm  $\text{Al}_{0.33}\text{Ga}_{0.67}\text{As}$  layers. The top and bottom electrodes are n-GaAs layers. The voltage  $V_g$  applied between the conducting n-GaAs layers drops in the insulating layer between them. The details on this sample can be found in Ref. [18]. In all experiments the sample is immersed in superfluid helium. We perform Kerr rotation and photoinduced reflectivity experiments, in which spin-polarized DXs are optically excited in the CQW by a circularly polarized pump pulse, Fig. 1 (b). The resulting dynamics of the spin polarization (density) is monitored via Kerr rotation (reflectivity) of the delayed linearly polarized probe pulse. Two-color measurements are realized by spectral filtering of pump and probe pulses with two  $4f$  zero-dispersion lines. The pulse duration is 1 ps, the spectral width is 1.5 meV. The Ti-Sapphire laser repetition rate is reduced to 20 MHz by a pulse-picker in order to avoid exciton accumulation between pulses. The laser spot diameter on the sample is 100  $\mu\text{m}$ , typical powers are 120 and 70  $\mu\text{W}$  for pump and probe, respectively [19].

The photoinduced reflectivity signal  $\delta R$  provides information on the total exciton density in the CQWs. Fig. 2 (a, b) shows  $\delta R$  measured as a function of the pump-probe delay  $\delta t$  and probe energy  $E_{pr}$ , at fixed pump energy  $E_{pp} = 1.568$  eV. These data show that even in the unbiased device the photoinduced reflectivity, and thus the exciton population persist as long as 5 ns. At short

pump-probe delays, a double resonance structure is apparent. In the biased structure (Fig. 2 (b)) the spectral profile of  $\delta R$  also changes significantly during the first nanosecond after the pump pulse. However, a strong signal persists at the longest delays studied. Decreasing the time interval between laser pulses from 48 ns to 24 ns leads to the accumulation of the excitons between pulses and the pump-probe signal at negative delays builds up. This means, that the life-time of excitons in this structure is of the order of 30 ns, consistent with the IX photoluminescence kinetics measurements [18].

Fig. 3 (c) shows typical time scans of the photoinduced reflectivity at three different values of the gate voltage and fixed probe energy, which show non-monotonous behavior. This non-monotonous behavior is due to the shift of the spectrum during the first nanosecond after the pump pulse (Fig. 2 (a, b)). At longer delays the decay becomes bi-exponential, with the characteristic times plotted in Fig. 3 (d) as a function of the gate voltage. While the shortest decay time  $\sim 1$  ns does not depend on the voltage, the longer decay time has a pronounced voltage dependence. The decay of the excitonic population is faster at  $V_g = 0.3$  V than the decay in the unbiased device.

The observed dynamics of the exciton population, as well as its voltage dependence can be understood as a footprint of both DXs and IXs, and their voltage-controlled anticrossing. Indeed, the exciton states in CQWs are formed from four possible electron-hole pair states. The corresponding exciton energies and oscillator strengths can be accurately calculated by solving Schrödinger equations [20]. The resulting DX-IX anticrossing is well described by the simple two-level anticrossing picture (Fig. 3 (a, b)). At  $V_g = 0$ , DX is the ground state of the system, IX is only several meV above it, and its oscillator strength is only 10 times smaller. In this case  $\delta R$  spectral shape exhibits the double resonance structure, with both DX and IX contributions (Fig. 2 (a)), and two decay times which differ by a factor of 10 (Fig. 3 (d)). By contrast, at  $V_g = 0.8$  V, the IX state is about 16 meV below the DX and has an oscillator strength 100 times smaller than DX. Thus, the fast decay of the  $\delta R$  signal is due to DX recombination, and slow relaxation is due to IXs recombination (Fig. 3 (d)). Remarkably, neither pump nor probe pulses are resonant with IX transition, so that the entire nonlinear signal results from DX-IX interaction. The smallest difference between the two decay times is observed at  $V_g = 0.3$  V, close to the DX-IX anticrossing point. The gate voltage dependence of the two decay times fits to the coupled oscillator model shown in Fig. 3 d. The complex spectral shape and dynamics of  $\delta R$  at short pump-probe delays is due to the high density of both DXs and IXs in the device, its detailed understanding is beyond the scope of this work.

Kerr rotation measurements provide the information

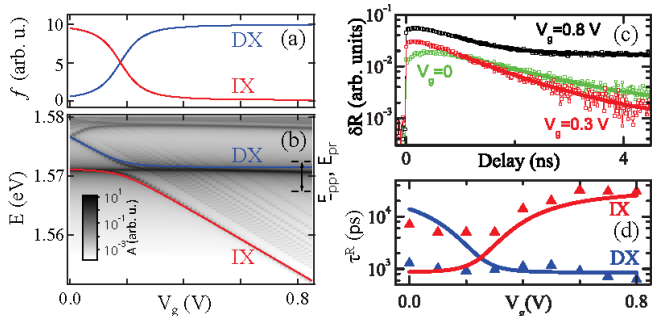


FIG. 3. (a) Oscillator strengths and (b) energies of DX and IX calculated from the coupled oscillators model as a function of the gate voltage. Color map in (b) shows accurate solution for excitonic absorption obtained from Schrödinger equation [20]. (c) Photoinduced reflectivity measured (symbols) as a function of  $\delta t$  at  $E_{pr} = 1.570$  eV, solid lines are fit to bi-exponential decay. Pump energy  $E_{pp} = 1.568$  eV. (d) IX and DX lifetimes extracted from bi-exponential fit of the reflectivity decay (symbols), and inverse oscillator strengths of DX and IX coupled oscillators (solid lines).

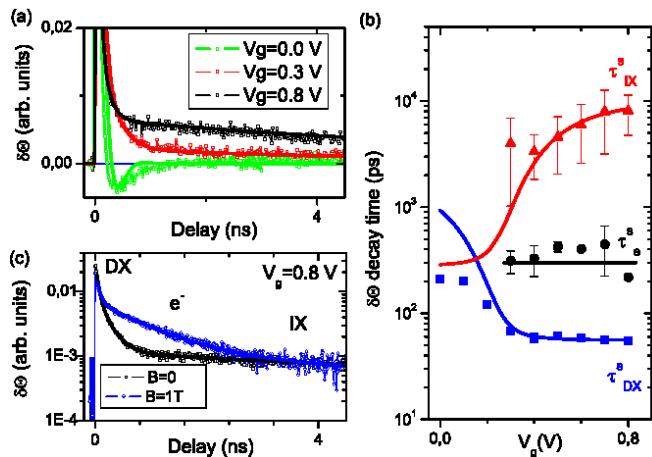


FIG. 4. (a) Photoinduced Kerr rotation (symbols) as a function of  $\delta t$  at  $E_{pr} = 1.569$  eV, solid lines are damped cosine ( $V_g = 0$ ) and triple exponential decay ( $V_g = 0.3$  and  $0.8$  V) fitted curves. Pump energy  $E_{pp} = 1.568$  eV. (b) Spin lifetimes extracted from Kerr rotation decay as a function of gate voltage (symbols). Solid lines: coupled oscillators model for DX and IX, estimation from Dyakonov-Perel mechanism for electrons. (c) Same as (a) in log scale at  $V_g = 0.8$  V,  $B = 0$  (black squares) and at  $B = 1$  T (blue circles). Solid lines are triple exponential decay fit to the data.

on the spin dynamics in CQWs and the results are even more intriguing (Fig. 2 (c, d)). At  $V_g = 0$  the rapid decay of  $\delta\Theta$  is accompanied by the inversion of the derivative-like spectrum at 0.5 ns. In contrast, at  $V_g = 0.8$  V the rapid decay is followed by much slower relaxation on the scale of several nanoseconds without the inversion of the spectrum. In Fig. 4 (a) we plot the Kerr rotation mea-

sured at fixed probe energy. At  $V_g = 0$  the signal is nonmonotonous, consistent with the spectrally resolved measurements of Fig. 2 (c). At higher voltages, the decay is triple exponential, with the longest spin lifetime reaching 10 ns. The decay times obtained by fitting the data at different gate voltages are summarized in Fig. 4 (b).

We propose the following interpretation of these observations. First of all, in semiconductor heterostructures a small splitting between two perpendicularly polarized linear exciton states  $\delta_{xy}$  is generally present [2]. The optical birefringence due to this splitting has been studied in detail in QW microcavity structures [21]. For an exciton spin this splitting acts as an effective in-plane magnetic field. Therefore, relaxation of the spin polarization is accompanied by its rotation around this effective field with an angular frequency  $\Omega_{xy} = \delta_{xy}/\hbar$ , provided that the precession is fast enough with respect to the exciton spin relaxation  $\Omega_{xy} > 1/\tau_s$ . Indeed, Kerr rotation at zero and small bias is well described by the damped cosine function (solid line), assuming the Gaussian distribution of precession frequencies centered at  $\omega = 6$  GHz (corresponding to  $\delta_{xy} = 4$   $\mu$ eV), with the standard deviation  $\sigma = \pm 2.5$  GHz, and the exciton spin relaxation time  $\sim 200$  ps. The latter is longer than DX spin relaxation expected in a single QW of the same width [9, 22]. The DX coupling to the energetically close IX state is probably responsible for this effect. Coherent rotation of the exciton, rather than an electron spin in the presence of the applied in-plane magnetic field have been observed in time-resolved PL experiments [23]. It was shown to be governed by the stability of the hole spin within the exciton. The hole spin relaxation time  $\tau_s^h$  should satisfy the condition  $1/\tau_s^h < \delta_{exc}/\hbar$ , where  $\delta_{exc}$  is the electron-hole exchange energy [24]. Assuming  $\delta_{exc} = 70$   $\mu$ eV in the unbiased structure [25] yields  $\tau_s^h > 10$  ps, which should be fulfilled in the studied structure under a low power excitation [26]. Application of the electrical bias reduces the exchange energy [27]. Indeed, at  $V_g > 0.2$  V the Kerr rotation decay becomes monotonous. At high voltages, the shortest decay time of order of 50 ps can be attributed to the polarization relaxation of DXs [9, 22]. The two other components have characteristic decay times of the order of 200 ps and several nanoseconds, respectively, the latter increasing with the gate voltage. They can be attributed to the spin relaxation of the 2DEG, which forms in biased CQWs [5, 10, 28], and IXs.

One of the main results of this work is the distinction between the spin polarized IXs and the spin polarized 2DEG traditionally studied by pump-probe Kerr rotation technique. The voltage dependence of the spin dynamics suggests, that fastest and slowest components are due to DX and IX, respectively. Indeed, we reproduce the voltage dependence of these two components within the model of the two coupled oscillators (solid lines in Fig. 4 (b)). By contrast, the electron spin relaxation is not expected to be voltage dependent, the

Rashba contribution to the spin-orbit field being small with respect to the Dresselhaus field [29, 30]. Within IXs we deal with the spin relaxation of an electron bound to the hole, but their exchange coupling is negligible at high  $V_g$ . The key parameter which controls the spin relaxation of electrons is the degree of their localization in the disorder potential [31]. Indeed, the electron spin relaxation time due to spin-orbit coupling can be written as  $\tau_s^e = (1 + \tau_0/\tau_c)/(\tau_c\Omega_{SO}^2)$  [32]. Here  $\tau_0$  is the characteristic time during which an electron remains localized and is not affected by the spin-orbit field,  $\tau_c$  is the correlation time of the spin-orbit field [33], and  $\Omega_{SO}$  is the spin-orbit frequency. Depending on the relative values of  $\tau_c$  and  $\tau_0$ , electrons (IXs) are either localized ( $\tau_c \ll \tau_0$ ), or mobile ( $\tau_c \gg \tau_0$ ). One can easily see that faster spin relaxation is expected for mobile, than for localized electrons [31, 32, 34]. Because an exciton is heavier than an electron, at low density it can be efficiently localized by the disorder potential, while at high density the mobility threshold can be reached [35]. To check this idea, we studied the power dependence of the Kerr rotation. Increasing the pump power allows to increase the IX density up to the mobility threshold, while keeping the electron density fixed. It turns out that the slow component disappears above a critical power [32]. This corroborates the interpretation of the slow component in terms of the spin polarization of the localized IX, which disappears above the mobility threshold. On the other hand, increasing excitation power results to a relatively weak gradual variation of the fast component that supports its assignment to the residual electron spin. Electron spin relaxation is accelerated due to the heating of the electron gas by the photogenerated carriers [36].

The ultimate test of this interpretation is the application of a longitudinal magnetic field, which suppresses spin relaxation of residual electrons much more efficiently, than that of the electrons bound to holes within IXs [32]. For electrons within IX the suppression factor is given by  $\tau_s^{e,B}/\tau_s^e = 1 + (\Omega_L\tau_c)^2$ , where  $\Omega_L$  is the Larmor frequency [37]. For the electrons which are not bound into the excitons and thus are subject to the cyclotron motion,  $\tau_s^{e,B}/\tau_s^e = 1 + (\Omega_c\tau_c)^2$ , where  $\Omega_c$  is the cyclotron frequency. Because the cyclotron frequency is usually higher than the Larmor frequency, spin relaxation of the free electrons is expected to be much strongly affected by the magnetic field. Moreover, since the same  $\tau_c$  is involved in the spin relaxation and its quenching in the presence of the magnetic field, measuring both times further tightens the conditions on the localization degree of both excitons and electrons. Fig. 4 (c) shows Kerr rotation at  $V_g = 0.8$  V as a function of the pump-probe delay at  $B = 0$  and  $B = 1$  T. Among the three decay components, only one with  $\tau_s^e = 200$  ps is affected by the magnetic field. A systematic study of the magnetic field effect shows that it increases by a factor of three for all  $V_g > 0.3$  V, as expected for the electrons, while

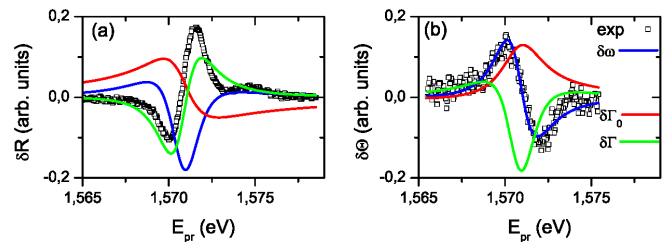


FIG. 5. Probe spectra of photoinduced reflectivity (a) and Kerr rotation (b) measured at 5 ns pump-probe delay,  $E_{pp} = 1.568$  nm (squares). Lines are calculated assuming photoinduced modification of the DX properties: energy blue shift (blue), saturation (red) and narrowing (green) [17].

slow component remains unchanged, as expected for IXs. The analysis of these results in the framework of the spin orbit relaxation model is reported in the Supplemental Material. It allows for the identification of the fast decay as being due to the spin relaxation of resident electrons, and the slow decay as being due to the localized IXs.  $\tau_s^{IX}$  reaches about 10 ns (Fig. 4 (c)), consistent with the polarization lifetime of localized IXs measured in PL imaging experiments [35].

Spectral analysis of the  $\delta R$  and  $\delta\theta$  provide important information on the excitonic nonlinearities. We focus here on the behavior at high voltages and long pump-probe delays, where the signal is dominated by IXs. Fig. 5 shows the spectra measured at  $V_g = 0.8$  V and  $\delta t = 5$  ns. To identify the dominant nonlinearity we follow the roadmap proposed in Ref. [17]. First of all we measure linear reflectivity in the vicinity of the DX resonance. The presence of IXs can modify the linear reflectivity via one of the three mechanisms: energy shift  $\delta\omega$ , saturation  $\delta\Gamma_0$  and narrowing/broadening of the resonance  $\delta\Gamma$  [17, 26, 38]. The spin independent mechanisms contribute to the photoinduced reflectivity only, while spin-dependent ones are responsible for the Kerr rotation. Fitting to the data in Fig. 5 (a) shows that the photoinduced reflectivity signal is dominated by the DX resonance narrowing. This can be understood as a reduction of the DX inhomogeneous broadening due to the screening of the QW disorder potential by localized IXs. Thus, at least at low IX densities, the impact of the DX blue shift due to the IX-DX interaction on the pump-probe spectra is weaker than that of the narrowing of the DX line. However, the blue shift of the DX resonance provides the main contribution to the Kerr rotation, Fig. 5 (b). This is consistent with a strong spin dependence of the DX blue shift [17].

In conclusion, we have shown that despite their vanishing oscillator strength, IXs in biased CQWs can be efficiently addressed by pump-probe spectroscopy. The detection of both photoinduced reflectivity and Kerr rotation provides a powerful tool for unraveling the spin



dynamics of IXs and the 2DEG, exploring IX-DX interaction and probing both bright and dark IX populations. In the appropriately chosen CQW devices, this method may help solving the challenging problems of the exciton physics, which are not easily accessible by other experimental means, such as determination of relative density and spin polarization of the bright and dark IX states.

*Acknowledgments.* We are grateful to K. V. Kavokin and M. I. Dyakonov for valuable discussions and ac-

knowledge the support of EU ITN INDEX PITN-GA-2011-289968. LVB was supported by DOE Award DE-FG02-07ER46449 and JRL by a Chateaubriand Fellowship. AK acknowledges the support from the Russian Ministry of Education and Science, Contract No 11.G34.31.0067. MN acknowledges the support from the Polish National Science Center under decision DEC-2013/09/B/ST3/02603.

---

## Supplemental Material

### DEPENDENCE OF THE INDIRECT EXCITON SPIN AND POPULATION ON THE PUMPING ENERGY AND POWER.

In this section we show that at given pumping power, the spin polarization of indirect excitons (IX) is optimized for the excitation energy slightly below DX resonance, and that this can be understood in terms of the density dependence of the exciton spin relaxation. Fig. S1 (a) shows Kerr rotation measured at  $V_g = 0.8$  V for two different excitation energies and same power  $P = 120$   $\mu$ W as the measurements shown in the main text. Probe energy is chosen to optimize the signal at 3 ns pump-probe delay. One can see, that under high energy pumping slow component of the Kerr signal disappears completely, so that no signal related to the IX spin dynamics can be identified. The energy of the pump beam with respect to the non-resonantly excited photoluminescence (PL) of the CQW device at the same gate voltage (black line) is shown in Fig. S1 (b). One can see, that the two pump energies are situated on the different sides of the DX emission line. For roughly 1 meV shift between DX absorption and emission and 1.571 eV corresponding to the absorption maximum [28], we argue that at  $E_{pp} = 1.571$  eV resonant excitation maximizes the IX density, while at  $E_{pp} = 1.568$  eV the IX density is much lower. This is unambiguously confirmed by resonant PL experiments for this two pump energies (Fig. S1 (b), green and red lines). The PL measurements are taken in exactly the same conditions as the pump-probe measurements. For the high energy excitation the IX emission is 3 meV above the IX emission at low energy excitation. The blue shift of the emission is a clear signature of the higher IX density  $n_{IX}$  and the resulting delocalization of IX, because the amplitude of the disorder potential is expected to be of order of 1 meV. In the framework of the plain capacitor model, the IX-IX interaction energy is given by  $u_0 n_{IX}$ , where  $u_0 = 4\pi e^2 d/\epsilon$ ,  $d$  is the separation between the QWs,  $e$  is the electron charge,  $\epsilon$  is the background dielectric constant [39]. From the measured blue shift this approximation gives for the studied structure under high energy excitation  $n_{IX} \simeq 2 \cdot 10^{10}$   $\text{cm}^{-2}$ , and not more than  $5 \cdot 10^9$   $\text{cm}^{-2}$  at low energy excitation.

In order to confirm further the role of the exciton density in the spin relaxation processes, we report in Fig. S2 the normalized excitation spectra of the Kerr rotation and reflectivity measured immediately after the excitation (pump-probe delay  $\delta t = 5$  ps) and at long delays  $\delta t = 5$  ns. The probe energy was fixed at  $E_{pr} = 1.57$  eV. One can see from the measurements at short delays, that the same pumping energy optimizes the carrier density ( $\propto \delta R$ ) and the spin density ( $\propto \delta \Theta$ ) created by the pump pulse. By contrast, at  $\delta t = 5$  ns the spin polarization is a trade off between the initial polarization and the spin relaxation rate. The spin polarization maximum is achieved at lower energy than the maximum of the IX population.

Finally, it's important to check, that lowering down the excitation power at  $E_{pp} = 1.571$  eV allows to recover the localization and slow spin relaxation of IXs. Fig. S3 shows power dependence of the Kerr rotation signal at  $V_g = 0.8$  V,  $E_{pp} = 1.571$  eV, solid lines are fits to bi- or three-exponential decay. With decreasing power, both electron and DX spin relaxation slow down progressively, but the slow component related to IX builds up only below the critical power (see inset of Fig. S3). This power should correspond to the IX density at which the IX-DX interaction energy is smaller than the disorder potential amplitude [7]. Thus we conclude that IXs spin dynamics is mainly determined by its localization degree, Dyakonov-Perel spin relaxation being abruptly quenched for the excitation powers below IX localization transition.

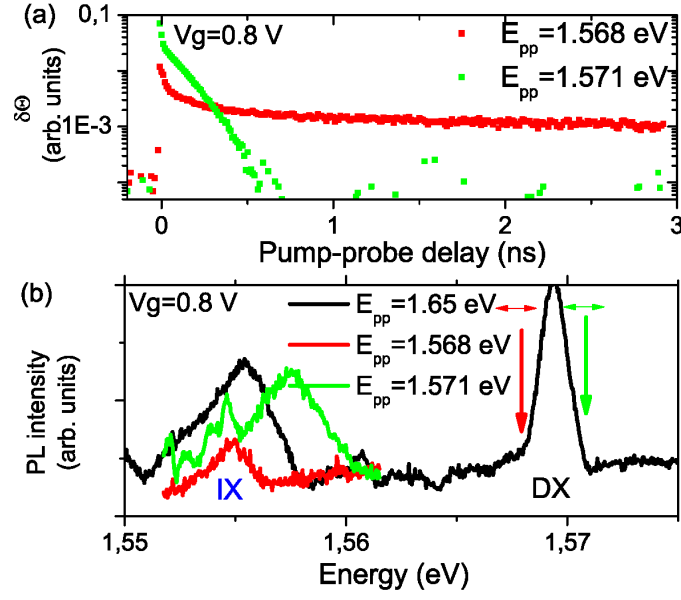


FIG. S1. (a) Photoinduced Kerr rotation as a function of pump-probe delay measured at  $E_{pp} = 1.569$  eV,  $V_g = 0.8$  V. Pump energies are  $E_{pp} = 1.568$  eV (red) and  $E_{pp} = 1.571$  eV (green). (b) Photoluminescence spectra measured at  $V_g = 0.8$  V for different excitation energies  $E_{pp}$ . IX emission is blue shifted at  $E_{pp} = 1.571$  eV (green) with respect to  $E_{pp} = 1.568$  eV (red) and non-resonant excitation  $E_{pp} = 1.65$  eV (black).

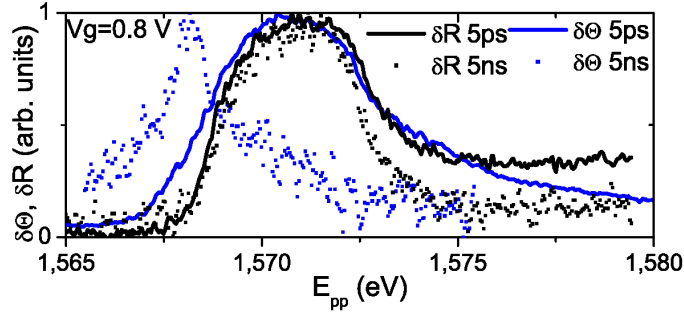


FIG. S2. Normalized Kerr rotation (blue) and photoinduced reflectivity (black) excitation spectra measured at  $E_{pp} = 1.57$  eV and  $V_g = 0.8$  V. Short pump-probe delay (5 ps, line) and long pump-probe delay (5 ns, symbols) are compared.

### MODEL FOR ELECTRON AND IX SPIN RELAXATION.

The key parameter which controls the spin relaxation of electrons is the degree of their localization in the disorder potential [31]. First of all in the regime of the strongest localization the spin relaxation of electrons is due to hyperfine interaction with a limited number of nuclear spins, which acts on the electron as a fluctuating effective magnetic field. This type of relaxation is typical for electrons localized in natural quantum dots, the characteristic spin decay time are on the scale of nanoseconds, and this relaxation is efficiently suppressed by the longitudinal magnetic field of the order of mT [40, 41]. In the experiments presented in this work long-living component of the spin polarization does not present any field dependence. Hence, we conclude that hyperfine field is not the main source of the spin relaxation in our CQWs, and will neglect the spin relaxation of localized electrons (IXs).

The other source of relaxation is the fluctuating effective magnetic field due to spin-orbit interaction. While an electron (or IX) hops from one localization site to another, its spin experiences random rotations. In bulk zinc blende crystals this mechanism is a major cause of spin relaxation for the localized states in the impurity-band [42]. In order to take into account the localization, we describe the diffusion of an electron (IX) in the QW in-plane disorder potential by two times. These are correlation time of the fluctuating spin-orbit field  $\tau_c$ , during which the spin-orbit field can be considered as constant, and  $\tau_0$ , during which an electron remains localized and not affected by the spin-orbit field. The strength of the spin-orbit interaction is given by the root mean square value of the electron Larmor frequency in

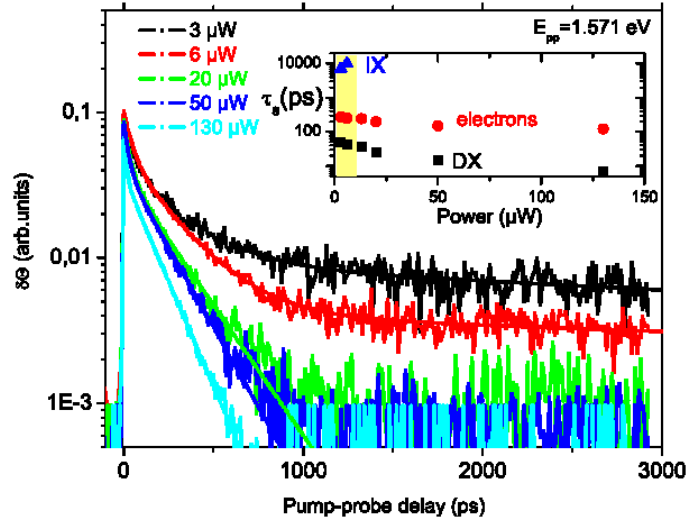


FIG. S3. Kerr rotation (symbols) measured as a function of the pump-probe delay at  $E_{pp} = 1.57$  eV,  $V_g = 0.8$  V. At typical pump power  $P_{pp} = 130$   $\mu$ W used throughout this work no long-living spin polarization is detected at the pump energy  $E_{pp} = 1.571$  eV. Lowering down the pump power allows to recover the slow component. Solid lines are fits to bi-exponential ( $P_{pp} = 130$  to  $P_{pp} = 20$   $\mu$ W) or tree-exponential ( $P_{pp} = 6$  and  $P_{pp} = 3$   $\mu$ W) decay. Inset: spin life-times of DXs, electrons and IXs extracted from the fits. The spin life-times in the yellow region are similar to the results obtained at  $E_{pp} = 1.568$  eV and  $P_{pp} = 130$   $\mu$ W, described in the main text.

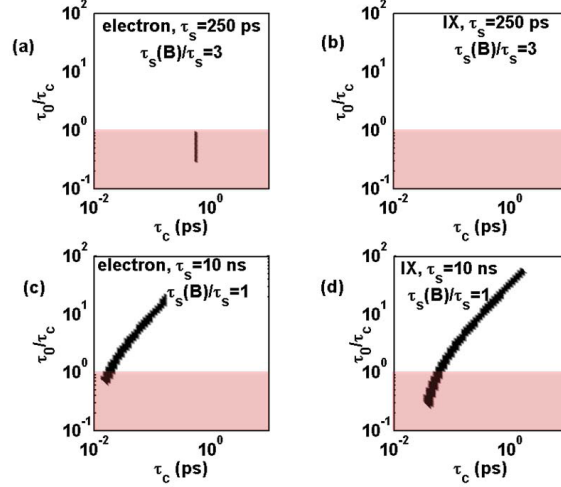


FIG. S4. The two components of spin polarization signal mapped on  $(\tau_c, \tau_0/\tau_c)$  parameter space. Pink areas denote the mobility area where  $\tau_c > \tau_0$ . Fast component ( $\tau_s = 250$  ps),  $\tau_s(B)/\tau_s = 3$ ) is calculated assuming either electron (a) or IX (b) spin relaxation. There are no points in the parameter space for the fast relaxation of IX. Slow component ( $\tau_s = 10$  ns),  $\tau_s(B)/\tau_s = 1$ ) can be obtained for both electrons (c) and excitons (d).

the spin-orbit field  $\Omega_{SO} = 2\beta k/\hbar$ , where  $\beta = 2$   $\mu$ eV $\cdot\mu$ m is the spin-orbit constant [29, 35] and  $k$  is the wave vector of the electron (IX). We shall assume that both residual electrons and electrons bound to holes within photoinduced IXs are characterized by their thermal wave vectors,  $k_e = 17$   $\mu$ m $^{-1}$ ,  $k_{IX} = 10$   $\mu$ m $^{-1}$  at  $T = 2$  K. If the in-plane motion of an electron (IX) consist in hopping between the localization sites, the well-known Dyakonov-Perel formula for the spin relaxation time [37] should be scaled by the factor  $1 + \tau_0/\tau_c$ , so that  $\tau_s^{e(IX)} = (1 + \tau_0/\tau_c)/(\tau_c \Omega_{SO}^2)$ . In the limit of free carriers ( $\tau_c \gg \tau_0$ ) this formula is reduced to the usual Dyakonov-Perel expression  $\tau_s^{e(IX)} = 1/(\tau_c \Omega_{SO}^2)$ . Note also, that both  $\tau_c$  and  $\tau_0$  depend on the carrier density and are *a priori* different for electrons and IXs in a CQW.

The longitudinal magnetic field affects differently the spins of residual electrons and the spins of electrons bound to holes within IXs. The precession of the electron spin in the longitudinal magnetic field averages out the random

effective field due to spin-orbit interaction during the correlation time  $\tau_c$ . The spin relaxation time in the presence of the magnetic field is given by  $\tau_s^{e(IX)}(B) = (1 + (\Omega_L \tau_c)^2) \tau_s^e$ , where  $\Omega_L$  is the Larmor frequency [37]. For the electrons which are not bound into the excitons and thus are subject to the cyclotron motion, an additional mechanism further suppresses the Dyakonov-Perel relaxation [43]. In this case, the field induced increase of the spin relaxation time is given by  $\tau_s^e(B) = (1 + (\Omega_c \tau_c)^2) \tau_s^e$ , where  $\Omega_c$  is the cyclotron frequency. Cyclotron frequency is two orders of magnitude higher than Larmor frequency so that spin relaxation of the free electrons is expected to be much stronger affected by the magnetic field.

Our strategy is to map both experimentally observed spin components ( $\tau_s = 250$  ps,  $\tau_s(B)/\tau_s = 3$  and  $\tau_s = 10$  ns,  $\tau_s(B)/\tau_s = 1$ ) to this model. Fig. S4 shows the result of such mapping for fast (a, b) and slow (c, d) components, assuming either electron (a, c) or IX (b, d) relaxation. Pink areas mark the mobility region where  $\tau_c > \tau_0$ . Dark lines show the results of the calculation of the ratio  $\tau_0/\tau_c$  which fit the experimental results, for each value of the correlation time. One can see that in Fig. S4 (b) there are no dark points at all. This means that the fast component is necessarily due to electrons, mainly because it is strongly affected by the magnetic field. These electrons are mobile, since  $\tau_c > \tau_0$ . By exclusion, the slow component should result from the spin relaxation of IX, which are essentially localized  $\tau_c < \tau_0$ .

- 
- [1] A. A. High, J. R. Leonard, A. T. Hammack, M. M. Fogler, L. V. Butov, A. V. Kavokin, K. L. Campman, and A. C. Gossard, *Nature* **483**, 584 (2012).
  - [2] A. A. High, A. T. Hammack, J. R. Leonard, S. Yang, L. V. Butov, T. Ostatnický, M. Vladimirova, A. V. Kavokin, T. C. H. Liew, K. L. Campman, and A. C. Gossard, *Phys. Rev. Lett.* **110**, 246403 (2013).
  - [3] M. Alloing, M. Beian, D. Fuster, Y. Gonzalez, L. Gonzalez, R. Combescot, M. Combescot, and F. Dubin, *cond-mat.quant-gas arXiv:1304.4101v2* (2014).
  - [4] L. V. Butov, A. C. Gossard, and D. S. Chemla, *Nature* **418**, 751 (2002).
  - [5] L. V. Butov, L. S. Levitov, A. V. Mintsev, B. D. Simons, A. C. Gossard, and D. S. Chemla, *Phys. Rev. Lett.* **92**, 117404 (2004).
  - [6] M. Stern, V. Umansky, and I. Bar-Joseph, *Science* **343**, 55 (2014).
  - [7] M. Remeika, J. C. Graves, A. T. Hammack, A. D. Meyertholen, M. M. Fogler, L. V. Butov, M. Hanson, and A. C. Gossard, *Phys. Rev. Lett.* **102**, 186803 (2009).
  - [8] Y. Shilo, K. Cohen, B. Laikhtman, K. West, L. Pfeiffer, and R. Rapaport, *Nat Commun* **4**, 2325 (2013).
  - [9] M. Z. Maialle, E. A. de Andrada e Silva, and L. J. Sham, *Phys. Rev. B* **47**, 15776 (1993).
  - [10] R. Rapaport, G. Chen, D. Snoke, S. H. Simon, L. Pfeiffer, K. West, Y. Liu, and S. Denev, *Phys. Rev. Lett.* **92**, 117405 (2004).
  - [11] O. L. Berman, G. Gumbs, and P. A. Folkes, *Solid State Communications* **150**, 832 (2010).
  - [12] J. M. Kikkawa, I. P. Smorchkova, N. Samarth, and D. D. Awschalom, *Science* **277**, 1284 (1997).
  - [13] M. Syperek, D. R. Yakovlev, A. Greilich, J. Misiewicz, M. Bayer, D. Reuter, and A. D. Wieck, *Phys. Rev. Lett.* **99**, 187401 (2007).
  - [14] M. T. Portella-Oberli, V. Ciulin, J. H. Berney, B. Deveaud, M. Kutrowski, and T. Wojtowicz, *Phys. Rev. B* **69**, 235311 (2004).
  - [15] A. Malinowski, R. S. Britton, T. Grevatt, R. T. Harley, D. A. Ritchie, and M. Y. Simmons, *Phys. Rev. B* **62**, 13034 (2000).
  - [16] A. Brunetti, M. Vladimirova, D. Scalbert, M. Nawrocki, A. V. Kavokin, I. A. Shelykh, and J. Bloch, *Phys. Rev. B* **74**, 241101 (2006).
  - [17] A. V. Nalitov, M. Vladimirova, A. V. Kavokin, L. V. Butov, and N. A. Gippius, *Phys. Rev. B* **89**, 155309 (2014).
  - [18] L. V. Butov, A. Imamoglu, A. V. Mintsev, K. L. Campman, and A. C. Gossard, *Phys. Rev. B* **59**, 1625 (1999).
  - [19] We have checked that reducing probe to pump power ratio does not change the signal dynamics.
  - [20] K. Sivalertporn, L. Mouchliadis, A. L. Ivanov, R. Philp, and E. A. Muljarov, *Phys. Rev. B* **85**, 045207 (2012).
  - [21] A. Brunetti, M. Vladimirova, S. Cronenberger, D. Scalbert, M. Nawrocki, and J. Bloch, *Superlattices and Microstructures* **41**, 429 (2007).
  - [22] T. C. Damen, K. Leo, J. Shah, and J. E. Cunningham, *Applied Physics Letters* **58**, 1902 (1991).
  - [23] T. Amand, D. Robert, X. Marie, M. Brousseau, P. Le Jeune, and J. Barrau, *Phys. Rev. B* **55**, 9880 (1997).
  - [24] M. Dyakonov, X. Marie, T. Amand, P. Le Jeune, D. Robert, M. Brousseau, and J. Barrau, *Phys. Rev. B* **56**, 10412 (1997).
  - [25] E. Blackwood, M. J. Snelling, R. T. Harley, S. R. Andrews, and C. T. B. Foxon, *Phys. Rev. B* **50**, 14246 (1994).
  - [26] L. V. Fokina, I. A. Yugova, D. R. Yakovlev, M. M. Glazov, I. A. Akimov, A. Greilich, D. Reuter, A. D. Wieck, and M. Bayer, *Phys. Rev. B* **81**, 195304 (2010).
  - [27] G. Aichmayr, M. Jetter, L. Viña, J. Dickerson, F. Camino, and E. E. Mendez, *Phys. Rev. Lett.* **83**, 2433 (1999).
  - [28] L. Butov, A. Imamoglu, K. Campman, and A. Gossard, *Journal of Experimental and Theoretical Physics* **92**, 260 (2001).
  - [29] K. Kavokin and M. Portnoi, *Semiconductors* **42**, 989 (2008).
  - [30] M. Studer, G. Salis, K. Ensslin, D. C. Driscoll, and A. C. Gossard, *Phys. Rev. Lett.* **103**, 027201 (2009).



- [31] Z. Chen, S. G. Carter, R. Bratschitsch, P. Dawson, and S. T. Cundiff, *Nat Phys* **3**, 265 (2007).
- [32] see Supplementary Material.
- [33] Correlation time of a fluctuating field is a time during which the field may be considered as constant. In the case of the spin-orbit field and mobile electrons it's given by the momentum scattering time, while in the hopping regime it's rather the time of flight.
- [34] R. I. Dzhioev, K. V. Kavokin, V. L. Korenev, M. V. Lazarev, B. Y. Meltser, M. N. Stepanova, B. P. Zakharchenya, D. Gammon, and D. S. Katzer, *Phys. Rev. B* **66**, 245204 (2002).
- [35] J. R. Leonard, Y. Y. Kuznetsova, S. Yang, L. V. Butov, T. Ostatnický, A. Kavokin, and A. C. Gossard, *Nano Lett* **9**, 4204 (2009).
- [36] E. A. Zhukov, D. R. Yakovlev, M. Bayer, M. M. Glazov, E. L. Ivchenko, G. Karczewski, T. Wojtowicz, and J. Kossut, *Phys. Rev. B* **76**, 205310 (2007).
- [37] M. I. Dyakonov, ed., *Spin Physics in Semiconductors*, Springer series in solid-state sciences (2008).
- [38] Z. Chen, S. G. Carter, R. Bratschitsch, and S. T. Cundiff, *Physica E: Low-dimensional Systems and Nanostructures* **42**, 1803 (2010).
- [39] A. L. Ivanov, *EPL (Europhysics Letters)* **59**, 586 (2002).
- [40] I. A. Merkulov, A. L. Efros, and M. Rosen, *Phys. Rev. B* **65**, 205309 (2002).
- [41] I. Y. Gerlovin, Y. P. Efimov, Y. K. Dolgikh, S. A. Eliseev, V. V. Ovsyankin, V. V. Petrov, R. V. Cherbunin, I. V. Ignatiev, I. A. Yugova, L. V. Fokina, A. Grelich, D. R. Yakovlev, and M. Bayer, *Phys. Rev. B* **75**, 115330 (2007).
- [42] K. V. Kavokin, *Semicond. Sci. and Technol.* **23**, 114009 (2008).
- [43] E. Ivchenko, *Sov. Phys. Solid State* **15**, 1048 (1976).